


## Article

# Effects of Severe Plastic Deformation and Subsequent Annealing on Microstructures of a Ni<sub>50.6</sub>Ti<sub>49.4</sub> Shape Memory Alloy

Jintao Zhang <sup>1</sup>, Shibo Wang <sup>1</sup>, Peng Hu <sup>1</sup>, Yu Zhang <sup>2</sup>, Hua Ding <sup>1,2,\*</sup> and Yi Huang <sup>3,4,\*</sup> <sup>1</sup> School of Materials Science and Engineering, Northeastern University, Shenyang 110819, China<sup>2</sup> Key Laboratory of Light Structural Materials of Liaoning Province, Northeastern University, Shenyang 110819, China<sup>3</sup> Department of Design and Engineering, Faculty of Science and Technology, Bournemouth University, Poole BH12 5BB, UK<sup>4</sup> Materials Research Group, Department of Mechanical Engineering, University of Southampton, Southampton SO17 1BJ, UK

\* Correspondence: dingh@smm.neu.edu.cn (H.D.); yhuang2@bournemouth.ac.uk (Y.H.)

**Abstract:** High-pressure torsion (HPT) was applied to the Ni<sub>50.6</sub>Ti<sub>49.4</sub> (at. %) alloy ingot up to 1/4, 2, 16, 32 and 48 turns under a pressure of 6.0 GPa. The samples were examined by X-ray diffraction (XRD), transmission electron microscope (TEM) and microhardness measurement. The results indicate that martensitic transformation and formation of amorphous phase occurred during the HPT process. As the HPT turns increased, the more the amorphous phase formed. The fraction of amorphization was analyzed based on the X-ray results. The microhardness increased with the HPT turns, which may be related to strain-induced martensite transformation, formation of the amorphous phase, increased dislocation densities and grain refinement. Differential scanning calorimetry (DSC) test revealed that shape memory alloys can be produced by HPT and post-HPT annealing from a NiTi ingot.

**Keywords:** NiTi alloy; high-pressure torsion; microstructure; mechanical property; phase transformation



**Citation:** Zhang, J.; Wang, S.; Hu, P.; Zhang, Y.; Ding, H.; Huang, Y. Effects of Severe Plastic Deformation and Subsequent Annealing on Microstructures of a Ni<sub>50.6</sub>Ti<sub>49.4</sub> Shape Memory Alloy. *Metals* **2024**, *14*, 184. <https://doi.org/10.3390/met14020184>

Academic Editor: Elena P. Ryklina

Received: 29 November 2023

Revised: 26 January 2024

Accepted: 29 January 2024

Published: 2 February 2024



**Copyright:** © 2024 by the authors. Licensee MDPI, Basel, Switzerland. This article is an open access article distributed under the terms and conditions of the Creative Commons Attribution (CC BY) license (<https://creativecommons.org/licenses/by/4.0/>).

## 1. Introduction

Shape memory alloy (SMAs) possess many good properties such as dimensional stability, shape memory properties, ductility and workability [1–4]. NiTi alloys are the most commercially viable SMAs and have been widely used in many practical applications. Since plastic deformation, such as dislocation slip and twinning, is irreversible, these plastic strains cannot be restored by heating. Therefore, it is important to increase the critical stress for slip to produce stronger SMAs. Among several methods to increase the strength of materials, such as grain refinement, work hardening and precipitation hardening, grain refinement is an effective way to improve both mechanical and functional properties of NiTi alloys [5].

There are some reports on the substantial grain refinement in NiTi alloys by severe plastic deformation (SPD) [6–17]. Among various SPD methods, high-pressure torsion (HPT) is the most effective technique to achieve grain refinement [12–17]. In recent years, many works were reported on the microstructural evolution during HPT processing of NiTi alloys. Pushin et al. [13] investigated the phase and structural transformation in Ni<sub>50.5</sub>Ti<sub>49.5</sub> alloy with a metastable B2-austenite structure during HPT. It was found that stress induced martensite transformation occurred during HPT processing. The fine structure of the B19' martensite and its evolution into nanocrystalline and, subsequently, amorphous state with different HPT turns was characterized. Prolpshkim et al. reported the weak stress-induced transformation in an equiatomic NiTi alloy during HPT [14]. However, there are no reports on stress-induced transformation in several NiTi alloys with austenite B2 structures under HPT [15–17].

In all reported works on HPT processing of NiTi SMAs, amorphous phase formed due to the severe plastic strains. In some cases, complete amorphization was observed [16,17], whereas partial amorphization was observed at the same strain in other cases [13,18]. The amorphization of NiTi alloys during HPT plays a significant role on the mechanical property enhancement of the alloys because the grain sizes developed from an amorphous state and crystallization during HPT are much smaller than those achieved by other deformation methods. It was revealed that initial microstructures of NiTi alloys exert marked effects on the microstructural evolution during the HPT processes [14]. In addition, alloying compositions, deformation temperature and pressure all affect the microstructure evolutions of NiTi alloys in SPD process [14,19]. There are some published works on the dynamic characteristics of amorphization during deformation processes in NiTi alloys. DSC and TEM methods were adopted to investigate a cold rolled NiTi binary alloy, and it was revealed that the volume fraction of the amorphous phase increased linearly with strains, where the strain was not very high ( $\sim 2.0$ ) [20]. XRD results were used to reveal the dynamic feature of amorphization in a NiTi binary alloy during HPT processing [14].

All published research on HPT processing of NiTi binary alloys has focused on the microstructure evolution of materials subjected to prior plastic deformation before HPT. There is no systematic study on the microstructure development in NiTi ingots, i.e., materials without any prior plastic deformation before HPT. Therefore, in this research, we aim to utilize the NiTi ingot as a starting material as we want to develop a new manufacturing route, such as the route from ingot directly to HPT processing and subsequent annealing (with the advantages of less procedures and short production time), for producing shape memory material. Furthermore, the coexistence of stress-induced transformation and amorphization during HPT processing are worth being investigated. And it is important to clarify the dynamics of amorphization in NiTi alloys as amorphization is a very important process for producing ultrafine-grained SMA alloy in the subsequent annealing process.

In the present work, NiTi alloy ingot was subjected to HPT processing up to 48 turns in order to obtain an ultrafine-grained microstructure after the post-HPT annealing. The occurrence of stress-induced transformation during HPT was investigated, and the dynamics of amorphization were evaluated quantitatively. The microhardness of the samples was measured and correlated with microstructure development. Through HPT processing and post-HPT annealing on the initial NiTi ingot, the processed NiTi alloy exhibits the transformation behavior.

## 2. Experimental Material and Procedures

A NiTi alloy with a nominal composition of Ni<sub>50.6</sub>Ti<sub>49.4</sub> (at. %) was chosen in the present work. The material was prepared using a vacuum induction furnace. After melting, the ingot was homogenized at 850 °C for 12 h. The as-homogenized state is denoted as as-received state in the following part of the manuscript. The NiTi disks for HPT processing were cut by a wire cutting machine with 10 mm in diameter and 0.7~0.8 mm in thickness. Pure Ti disk shape foils with a thickness of 0.1 mm were put on top and beneath the NiTi disk before loading them as a whole piece into HPT anvils. HPT processing was conducted at room temperature under a pressure of 6.0 GPa and with a rotational speed of 1 rpm. NiTi ingot samples were processed up to 1/4, 2, 16, 32 and 48 turns. The equivalent strain in processed samples can be estimated using the following two equations [21]:

$$\gamma = \frac{2N\pi r}{h} \quad (1)$$

$$\varepsilon = \frac{2}{\sqrt{3}} \ln \left( \frac{\gamma}{2} + \sqrt{1 + \frac{\gamma^2}{4}} \right) \quad (2)$$

where  $r$  is the distance from the disk sample center,  $N$  is the number of revolutions,  $\gamma$  and  $\varepsilon$  are the shear strain and equivalent strain, respectively, and  $h$  is the final thickness of the HPT-processed sample. The calculated equivalent strains of samples with different HPT

turns along the disk sample radius direction are plotted in Figure 1. The equivalent strain increased from the disk sample's center to the edge area. Moreover, the equivalent strain increased with increasing HPT turns.

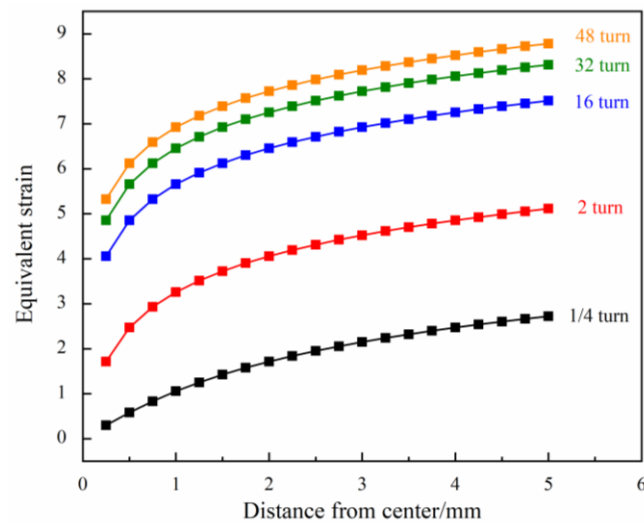


**Figure 1.** Calculated equivalent strain distribution along the radius direction in samples with different HPT turns.

Following HPT processing, annealing (450 °C for 2 h) was applied to the HPT-processed NiTi samples and then water quenched.

The samples for XRD examination were extracted from the disk samples by a wire-cutting machine and then mechanically ground. The XRD examination was conducted on Smart Lab 9 kW with a target of Cu. The angle of X-ray diffraction profiles was recorded through  $\theta$ - $2\theta$  scans from 10° to 90°, and the XRD scanning speed was 5°/min. The multi-peak fitting using the Gaussian peak function was processed and the second iteration carried out until the convergence was reached, full width at half maximum (FWHM) values of B2 (110) peak being attained.

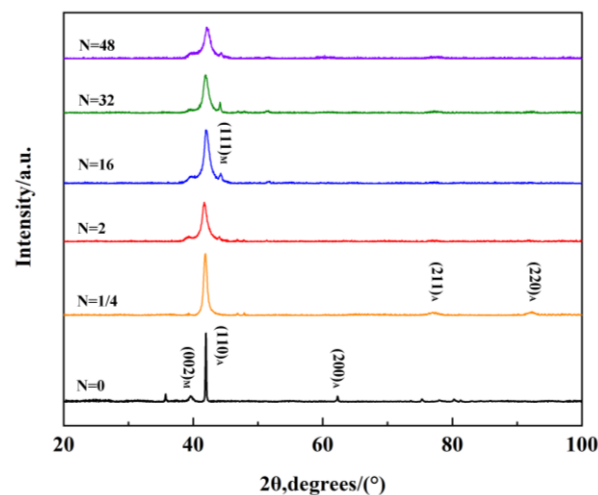
Vickers microhardness of NiTi samples was measured using an FM-700 tester, with a load of 0.5 kg force and dwell time of 10 s [22].

The transmission electron microscope (TEM) samples with 3 mm in diameter were cut off from the HPT samples by a wire-cutting machine. The samples were ground to a thickness of 50  $\mu\text{m}$  and then processed by the twin-jet electropolishing equipment TenuPol-5 (Struers). The electropolishing solution was  $\text{HClO}_4:\text{C}_2\text{H}_5\text{OH} = 1:9$ . After twin-jet electropolishing, the samples were carefully polished by ion beam using the equipment Gatan 695. The samples were firstly polished with an angle of  $\pm 5^\circ$  at the working voltage of 4.5 keV; and then, with the angle of  $\pm 4.5^\circ$  at the working voltage of 4.2 keV. The microstructures of the HPT-processed samples were examined by TEM equipment FEI G 20 (ThermoFisher Scientific, Waltham, MA USA).

### 3. Results

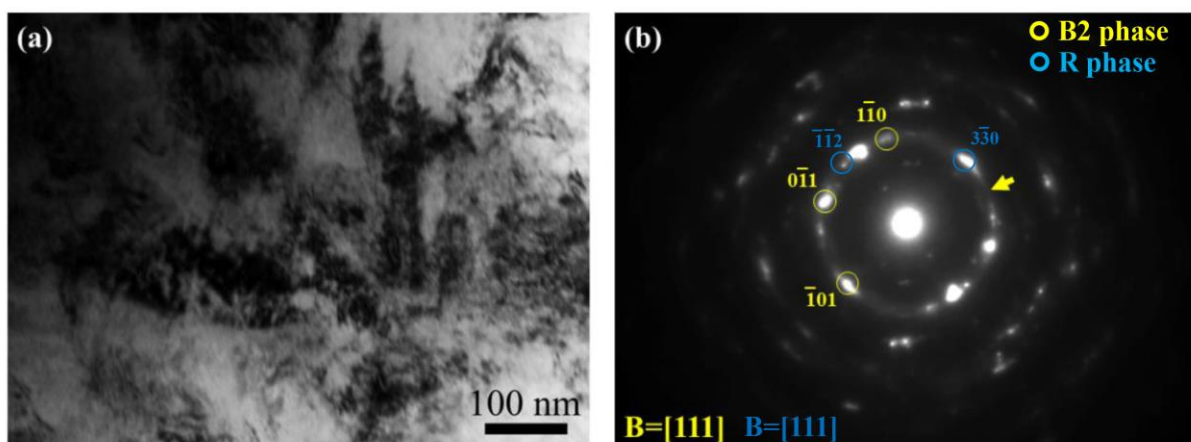
#### 3.1. Microstructure Characterization

Figure 2 shows the XRD patterns of the as-received sample and samples after different turns of HPT processing. The as-received microstructure was basically austenite. The main peak is  $(110)_\gamma$ , and other austenite peaks are  $(200)_\gamma$ ,  $(211)_\gamma$  and  $(220)_\gamma$ . New martensite peak  $(111)_\text{M}$  appeared near the main peak as the HPT turns increased to 2, which means the martensite B2-B 19' transformation arose. It was noticed that after HPT processing, line broadening of diffraction peaks occurred. In the as-received (denoted as N = 0 in Figure 2) and 1/4-turn samples, the XRD peaks are quite sharp, while the broadening of the diffraction peak becomes more obvious as the number of HPT turns increases, indicating the grain refinement and the increment of amorphous phase.



**Figure 2.** XRD spectrum of  $\text{Ni}_{50.6}\text{Ti}_{49.4}$  alloy prior to and after HPT.

The deformed microstructure in the 2-turns HPT sample is shown in Figure 3a. We can observe the dense dislocations in Figure 3a due to severe shear strain induced by HPT processing. The selective area electron diffraction (SAED) pattern in Figure 3b can verify the existence of austenite. It should be noted that the intermediate martensite, i.e., R phase, can also be verified by the SAED pattern in Figure 3b, showing that deformation-induced martensitic transformation occurred during HPT process. Meanwhile, the halo rings in the SAED in Figure 3b demonstrate the formation of the amorphous phase in the 2-turns HPT sample.



**Figure 3.** TEM microstructures of 2-turns HPT-processed  $\text{Ni}_{50.6}\text{Ti}_{49.4}$  sample. (a) Bright field image; (b) SAED.

The deformed microstructure in the 2-turns HPT sample is shown in Figure 3a. We can observe the dense dislocations in Figure 3a due to severe shear strain induced by HPT processing. The selective area diffraction pattern (SAED) in Figure 3b can verify the existence of austenite. Meanwhile, the halo rings in the SAED in Figure 3b (marked by the yellow arrow) demonstrate the formation of the amorphous phase in the 2-turns HPT sample. In fact, XRD results in Figure 2 also indicate the formation of martensite in the 2-turns HPT sample.

Figure 4 shows the microstructure development in the 16-turns HPT sample. The microstructure of position A in Figure 4a and the corresponding SAED pattern in Figure 4b show the deformed austenite along with dense dislocations. In addition, because of the severe plastic strain introduced by 16-turns HPT, the formation of the amorphous phase is verified by the halo in the diffraction patterns (Figure 4b, marked by the yellow arrow).

The microstructure of position B in Figure 4a and the corresponding SAED pattern in Figure 4c demonstrate that deformation-induced martensite transformation occurred in the 16-turns HPT sample and the martensite at position B has the feature of nano-scaled lath-typed microstructure.

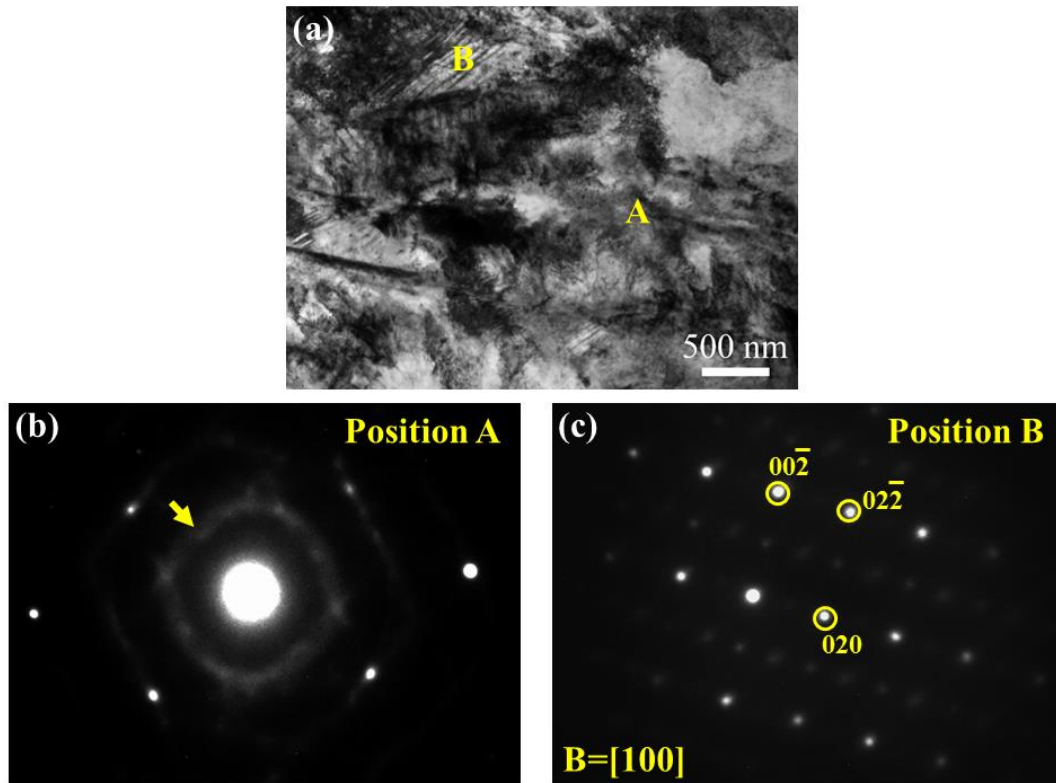


**Figure 4.** TEM microstructures of the 16-turns HPT-processed  $\text{Ni}_{50.6}\text{Ti}_{49.4}$  sample. (a) Bright image; (b) SAED of area A; (c) SAED of area B.

After 32 turns of HPT, more nano-scaled martensite lath can be observed (Figure 5a, marked by the red arrow) and more amorphous phase is exhibited according to the SAED pattern (Figure 5b, marked by the yellow arrow).

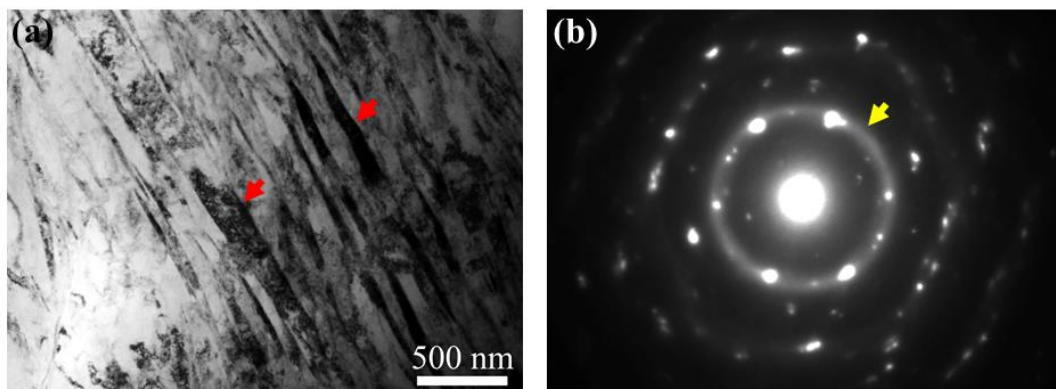


**Figure 5.** TEM microstructures of the 32-turns HPT-processed  $\text{Ni}_{50.6}\text{Ti}_{49.4}$  sample. (a) Bright field image; (b) SAED.

### 3.2. Microhardness Evolution

Figure 6 shows the microhardness evolution in the as-received and HPT-processed samples. The microhardness of the as-received sample is about 290 HV (denoted as

0 turns in Figure 6). The microhardness of the samples increases with HPT turns. The microhardness (HV) distributions along the radius of HPT-processed disk samples showed that the maximum value of HV is attained at the edge and the minimum value in the center part of the samples. The microhardness of the 1/4-turn sample increased to the average value of 355 HV, with 311.4 HV in the center and 465.4 HV at the edge. After 16 turns of processing, the sample had an average value of 398 HV, with 486.4 HV at the edge and 354.7 HV in the center. When the HPT turn increased to 48, the average value reached 442.1 HV, in which the microhardness at the edge and in the center was 546.26 HV and 368.69 HV, respectively.

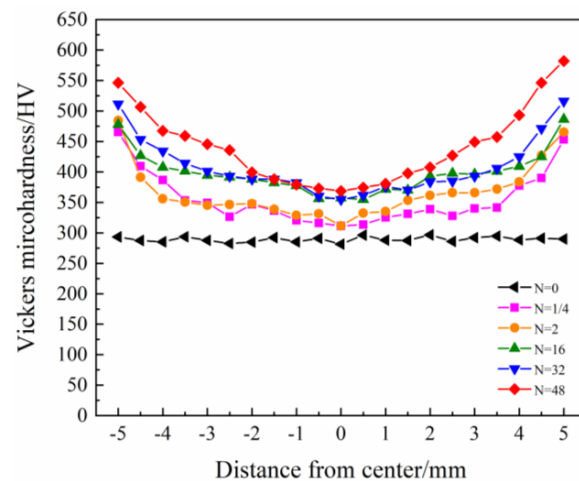


**Figure 6.** Microhardness of the samples prior to and after HPT.

### 3.3. Microstructure after Post-HPT Annealing

The microstructures of samples subjected to 1/4- and 16-turns HPT and post-HPT annealing are shown in Figures 7 and 8, respectively. Figure 7a shows lath-like microstructure features presented in the sample with 1/4-turn + post-HPT annealing, and the SAED pattern in Figure 7b confirms these are austenite grains. These lath-like austenite might result from the reverse martensite to austenite transformation during the post-HPT annealing process. In addition, the R phase can also be verified by the SAED pattern in Figure 7b, and the results show that B2 and R dual phases co-exist after 1/4-turn HPT + post-HPT annealing. After 16-turns HPT and subsequent annealing, refined and equiaxed grains in nano-scale formed, as shown in Figure 8a,c. Meanwhile, Figure 8b,d demonstrate that there still exists an R phase and lath-like austenite, which can also be evidenced by the DSC results in Figure 9.

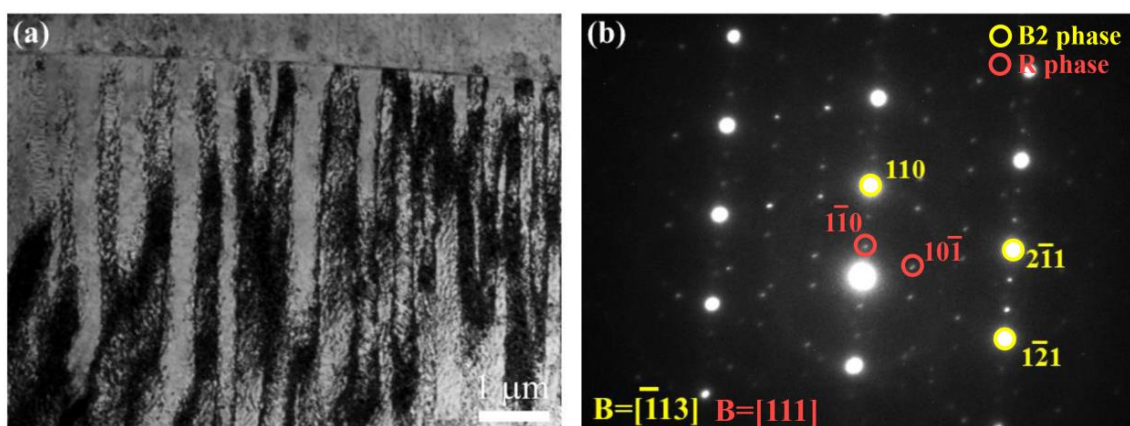


**Figure 7.** TEM microstructure of the  $\text{Ni}_{50.6}\text{Ti}_{49.4}$  sample after 1/4-turn HPT and subsequent annealing (450 °C for 2 h). (a) Bright field image; (b) SAED pattern.

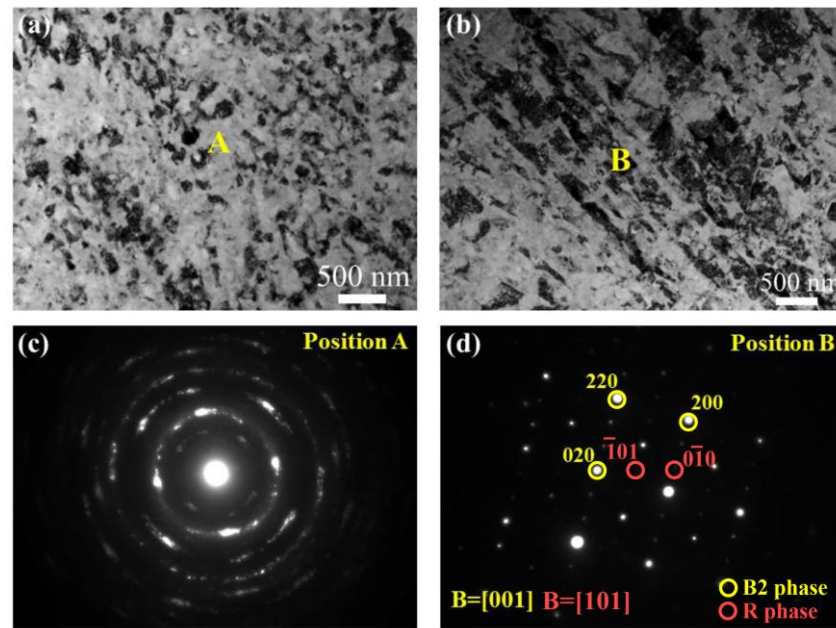


**Figure 8.** TEM microstructures of the  $\text{Ni}_{50.6}\text{Ti}_{49.4}$  sample after 16-turns HPT and subsequent annealing ( $450\text{ }^{\circ}\text{C}$  for 2 h). (a) Refined microstructure; (b) lath-like austenite; (c) SAED of area A; (d) SAED of area B.

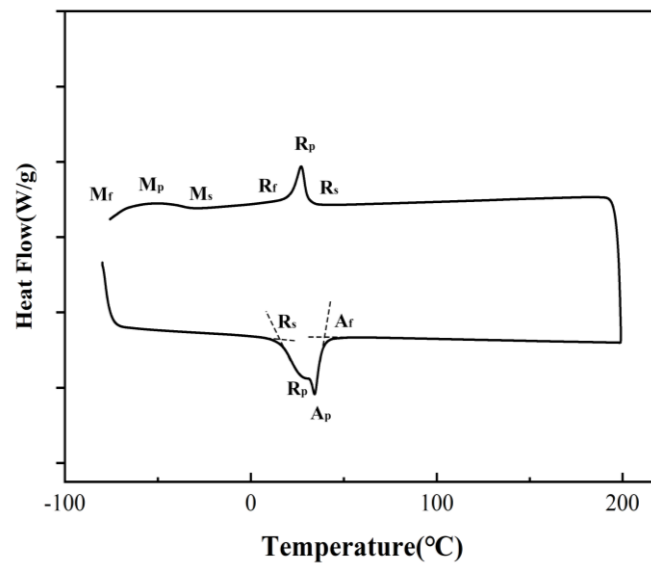


**Figure 9.** DSC results of  $\text{Ni}_{50.6}\text{Ti}_{49.4}$  sample after 16-turns HPT and subsequent annealing ( $450\text{ }^{\circ}\text{C}$  for 2 h).

### 3.4. Phase Transformation Behavior

Figure 9 shows the DSC results of the 16-turns HPT sample with post-HPT annealing at  $450\text{ }^{\circ}\text{C}$  for 2 h. It can be seen that the  $\text{B19}' \rightarrow \text{R} \rightarrow \text{B2}$  two-step phase transformation presented in the heating process, whereas the  $\text{B2} \rightarrow \text{R} \rightarrow \text{B19}'$  two-step phase transformation occurred during the cooling process. It is noticed that  $\text{B19}' \rightarrow \text{R}$  and  $\text{R} \rightarrow \text{B2}$  stages are not separated, but proceed continuously, and correspondingly, overlapping of their endothermic peaks is clearly observed in the DSC heating curve. The existence of an R phase could also be confirmed by the TEM results in Figure 8.

## 4. Discussions

### 4.1. Microstructural Evolution during HPT Processing

In severe plastic deformation, materials deviate from equilibrium states and various microstructural evolution features appear. Stress-induced martensite transformation and amorphization are the two processes that can occur in SPD-processed NiTi alloys.

In the present case, it was noticed that martensite transformation occurred in the 2-turns HPT sample when the shear strain was relatively small (deduced from the XRD results in Figure 2). In the 16- and 32-turns samples, a certain amount of martensite can be observed from the TEM observations (Figures 3 and 4), indicating the stress-induced transformation was quite active. The factors influencing the stability of austenite include compositions, grain size, grain morphology and densities of lattice defects. The containment of martensite in samples with relatively high HPT turns may be partly due to the large grain size of the initial material which was only homogenized without further plastic working. As the strains increased, a long-range stress field was built up by the high density of dislocations, which stabilized the B2 phase with respect to B19' martensite, and then deformation would concentrate in the austenite phase [23]. It is interesting to note that the intermediate R phase appears during HPT, which is seldom reported. As an intermediate phase, R-phase usually forms during cooling processes. R-phase transformation is a martensite transformation itself which competes with the subsequent martensite transformation. It is necessary to conduct a further investigation in the formation mechanism of the R phase of NiTi SMA in severe plastic deformation.

NiTi alloy is known to be susceptible to amorphization under shear deformation. The structural refinement by heavy deformation and amorphization combined with adequate heat treatment could lead to the improvement of shape memory characteristics [24,25].

The variations of amorphous volume fractions with true strain were investigated by DSC and TEM in NiTi alloys [20]. It was revealed that for equal nominal strain, the amorphous volume fractions were different for compression and cold rolling, and the linear relationship was demonstrated for both cases. It should be pointed out that dynamic features of amorphous transformation might not obey the linear relationship when the strains are large during SPD processes. However, there is a lack of quantitative description about the dynamic feature of amorphization during heavy deformation of NiTi alloys.

The measurement of X-ray line width allows an integral estimation of the structure [14]. The  $\{110\}_{B2}$  X-ray line half-width  $B$  vs.  $N$  and  $\varepsilon$  are shown in Table 1. If we adopt the half-width of the  $\{110\}_{B2}$  X-ray line as the indication of the amorphization of the material during HPT, it can be clearly seen that the fraction of the amorphous phase increases with strain. Furthermore, the kinetics of  $B$  change with strain is in a non-linear style, shown in Figure 10. When the strain was less than 4.3, the quick amorphization was exhibited while the rate of amorphization decreased afterwards.

**Table 1.** Values of FWHM of the diffraction peak corresponding to B2(110) plane of NiTi alloy with different conditions.

Number of Revolutions, N	Equivalent Strain, $\varepsilon$ (1/2 Radius)	FWHM, $2\theta$ °
0	0	0.15
1/4	1.952	0.59
2	4.313	0.85
16	6.714	0.95
32	7.514	1.04
48	7.983	1.22



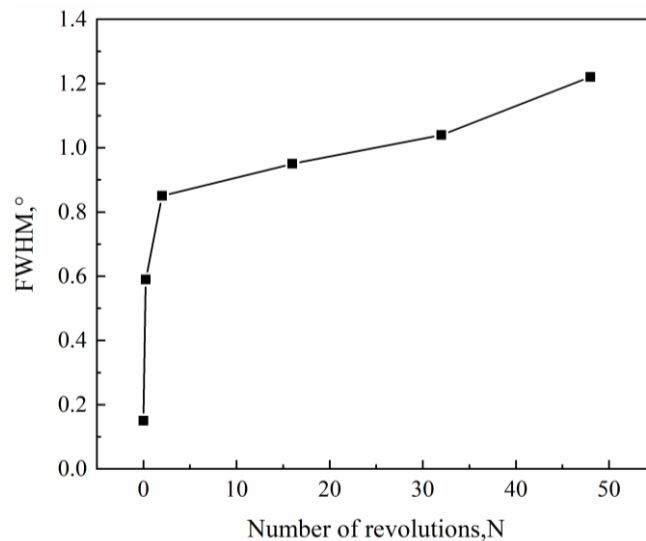


**Figure 10.** Variations of values of FWHM of the diffraction peak corresponding to B2(110) plane of NiTi alloy with number of revolutions.

The amorphization of NiTi alloys with different initial structures during HPT has been compared. Khmelevskaya et al. [19] found that the characteristics of structure formation in HPT-processed Ti-Ni-based alloys depend on widely varied composition, deformation temperature and pressure. They pointed out that the tendency to form an amorphous structure during SPD depends on relative positions of  $M_s$  and deformation temperature, and easier amorphization of martensite than austenite is due to the former having more lattice defects. They reported that the sample with martensite matrix exhibits the highest fraction of amorphous phase, the one with austenite matrix the least, and the one with a metastable microstructure is in the middle. As aforementioned, both stress-induced transformation and amorphization occurred in the present case. As seen from the XRD results (Figure 2), it seems that the amount of martensite phase increased from 2 to 32 turns and decreased when the HPT turn reached 48 turns. The formation of stress-induced martensite might cause stress concentration, which increases the stability of austenite, so that the transformation was limited to some extent. Increased dislocation density and refined grain boundaries both provide the energies for the initiation of amorphization [17]. With the increase in HPT turns, the accumulated dense dislocations provide the driving force for the amorphization process. As it is easy for amorphization to occur in martensite, the amorphous phase might also nucleate in the newly formed martensite. Therefore, the fraction of martensite no longer increased but even decreased when the strain was especially large.

Generally, the extent of amorphization is related to grain structures in the as-received state, alloy compositions, and processing parameters. It is noticeable that the amorphization during the HPT process in the current research is not very severe compared with the ones in other alloys with similar compositions under HPT [14–17]. The energy stored in the grain boundaries was estimated, and it was concluded that the grain boundaries and dislocations both contribute significantly to driving the crystalline to amorphous transformation [15]. This can explain why the amorphization is not severe in the present homogenized NiTi ingot with less boundaries and not many dislocations before HPT.

It can be seen from Figure 6 that the microhardness of the investigated NiTi alloy increases obviously after HPT processing. There are several factors which affect the mechanical properties of the investigated material. Strain-induced martensite transformation, introduction of densely populated dislocations, the formation of amorphous phase and microstructural refinement all contribute to the enhancement of the microhardness of the material.

In most HPT studies in NiTi alloys, amorphization has been paid much attention, while strain-induced martensite transformation was not emphasized to some extent. Since the as-received material in the present case is a homogenized ingot, amorphization is not as important as in the materials with fine initial microstructure, the strain-induced martensite and dislocations induced during the severe plastic deformation may have played important roles in the increase of mechanical properties during HPT.

#### 4.2. Microstructural Evolution after Post-Deformation Annealing

In previous studies, the as-received materials are mostly deformed microstructure with an austenite size of 30~50  $\mu\text{m}$  [13,16]. In the present study, the original one was a homogenized ingot. It was revealed that the grains were refined substantially after HPT processing and annealing treatment. Therefore, the combination of HPT and annealing is a very powerful way to gain fine-grain structures. The DSC results indicate that NiTi SMA can be produced by HPT and post-deformation annealing from an ingot.

The crystallization processes in amorphous materials provide interesting aspects of solid-state transformation under non-equilibrium conditions. The crystallization of an amorphous NiTi alloy should include nucleation and growth process, which is dependent on the annealing temperature and time. Two conditions should be met in order to obtain fine-grain structures, i.e., high nucleation rate and low growth rate. In HPT processing, there exist residual high-density defects which could provide sites for nucleation. The stored energy could be released during the annealing process and fine grains could be formed. Nano-scale structure with crystallization was achieved after post-HPT annealing (Figure 8). As seen in Figures 4 and 5, martensite laths formed during HPT and reverse transformation occurred during the annealing process (Figure 8). As the width of martensite laths was quite small, the reversed one was also quite fine. During the heat treatment, recrystallization also occurred as the temperature was in the recrystallization range of the alloy. Due to the large strains in the process and the high stored energy induced in HPT, the recrystallized grains must be quite small. An intermediate phase, R-phase, was also found. Multiple mechanisms appear in the HPT process; therefore, the microstructural evolution during the annealing process is complex in the investigated material.

#### 4.3. Transformation Behavior

Transformation temperature of NiTi alloys depends mainly on compositions and grain sizes of the materials. In the present work, the 16-turns sample was annealed to study the transformation behavior. In both heating and cooling processes, two-step transformation was found, R phase being exhibited. It was indicated that R phase appears as an intermediate phase, which was reported in many previous studies [26–30]. As the lattice distortion associated with the R-phase transformation (around 1%) is much less than the associated with B19' transformation (around 10%), the transformation path sometimes changes from B2→B19' into B2→R→B19', minimizing the transformation strain and interface energies that are opposing the transformation [27,29]. The R-phase transformation can be induced by various treatments, including thermal cycling, post-deformation annealing, aging and addition of ternary elements [26]. In coarse-grained structures, a single step transformation from B2 austenite to monoclinic B19' martensite is exhibited [27], whereas two-step martensite transformation usually occurs in cooling processes in nano-NiTi alloys [29,30]. In the present case, although the grain size of the initial microstructure was quite large, the microstructure was substantially refined after HPT. Therefore, two-step transformation appeared in the samples after the annealing treatment.

Severe plastic strains and heat treatment schedules have obvious impacts on the transformation behavior of NiTi-based alloys. A good balance of mechanical property and transformation behavior could be achieved by proper control of the deformation and annealing schedule. In the present study, NiTi SMA with an ultrafine-grained microstructure was successfully conducted via HPT and post-annealing on the NiTi ingot, which provides a more efficient route to fabricated ultrafine-grained NiTi SMA. Meanwhile, it should be

noted that if the microstructure of the as-received ingots is refined and homogenized to some extent, the mechanical properties of the NiTi SMA could be further increased.

## 5. Conclusions

1. During HPT processing of Ni<sub>50.6</sub>Ti<sub>49.4</sub> (at.%) alloy, stress-induced phase transformation and amorphization occurred. As the HPT turns increased, the fraction of the amorphous phase increased with a non-linear style. In the early stage of HPT, the rate of amorphization was quite fast, whereas it became moderate after 2 turns.
2. The microhardness was 290 HV in the as-received status. After 1/4-turn HPT, the average microhardness increased to 355 HV, and it increased to 398 HV when the HPT turns were 16. The increment of microhardness is due to the contributions from the strain-induced martensite transformation, the formation of the amorphous phase, increased dislocations and grain refinement.
3. After the HPT-processed 16-turns sample was annealed at 450 °C for 2 h, nano-scale grains were formed. DSC results revealed that SMA effect was exhibited in the post-HPT-annealed 16-turns sample. The results in the present work indicate that NiTi SMA can be produced directly from ingot by HPT and post-HPT annealing, which is a feasible processing route. The future direction is to achieve refined and homogeneous microstructure in NiTi ingots through HPT so that better mechanical properties can be achieved.

**Author Contributions:** Conceptualization, J.Z., H.D., S.W. and Y.H.; methodology, J.Z., H.D., S.W., P.H. and Y.Z.; investigation, J.Z., S.W., P.H. and Y.Z.; writing—original draft preparation, J.Z., H.D., S.W. and Y.H.; writing—review and editing, J.Z., H.D. and Y.H. All authors have read and agreed to the published version of the manuscript.

**Funding:** This research received no external funding.

**Data Availability Statement:** The raw data supporting the conclusions of this article will be made available by the authors on request.

**Conflicts of Interest:** The authors declare no conflict of interest.

## References

1. Jani, J.M.; Leary, M.; Subic, A.; Gibson, M.A. A review of shape memory alloy research, applications and opportunities. *Mater. Des.* **2014**, *56*, 1078–1113. [[CrossRef](#)]
2. Yana, B.; Zhang, Y.Q.; Jiang, S.Y.; Yu, J.B.; Sun, D.; Tang, M. Mechanical properties and fracture mechanisms of martensitic NiTi shape memory alloy based on various thermomechanical-processing microstructures. *J. Alloys Compd.* **2021**, *883*, 160797. [[CrossRef](#)]
3. Sun, D.; Jiang, S.Y.; Zhang, Y.Q.; Yan, B.Y.; Yu, J.B. Influence of annealing on incomplete detwinning and deformation twinning in equiatomic NiTi shape memory alloy undergoing severe plastic deformation. *J. Alloys Compd.* **2021**, *871*, 159550. [[CrossRef](#)]
4. Tadayyon, G.; Guo, Y.; Mazinani, M.; Zebbarjad, S.M.; Tierman, P.; Tofail, S.A.M.; Biggs, J.P. Effect of different stages of deformation on the microstructure evolution of Ti-rich NiTi shape memory alloy. *Mater. Charac.* **2017**, *125*, 51–68. [[CrossRef](#)]
5. Chen, H.; Xiao, F.; Liang, X.; Li, Z.X.; Li, Z.; Jin, X.J.; Min, N.; Fukuda, T. Improvement of the stability of superelasticity and elastocaloric effect of a Ni-rich Ti-Ni alloy by precipitation and grain refinement. *Sci. Mater.* **2019**, *162*, 230–234.
6. Zhang, J.T.; Wang, S.B.; Hu, P.; Zhang, Y.; Ding, H.; Huang, Y. A novel strategy for fabricating phase transforming NiTi shape memory alloy via multiple processes of severe plastic deformation. *Mater. Lett.* **2024**, *15*, 135439. [[CrossRef](#)]
7. Wang, Z.; Chen, J.; Kocich, R.; Tardif, S.; Dolbnya, I.P.; Kunčická, L.; Micha, J.S.; Liogas, K.; Magdysyuk, O.V.; Szurman, I.; et al. Grain structure engineering of NiTi shape memory alloys by intensive plastic deformation. *ACS Appl. Mater. Interfaces* **2022**, *14*, 31396–31410. [[CrossRef](#)]
8. Kreitchberg, A.; Brailovski, V.; Prokoshkin, S.; Gunderov, D.; Khomutov, M.; Inaekyan, K. Effect of the grain/subgrain size on the strain-rate sensitivity and deformability of Ti-50 at% Ni alloy. *Mater. Sci. Eng. A* **2015**, *622*, 21–29. [[CrossRef](#)]
9. Yan, B.Y.; Jiang, S.Y.; Sun, D.; Wang, M.; Yu, J.B.; Zhang, Y.Q. Martensite twin formation and mechanical properties of B2 austenite NiTi shape memory alloy undergoing severe plastic deformation and subsequent annealing. *Mater. Charac.* **2021**, *178*, 111273. [[CrossRef](#)]
10. Jiang, S.Y.; Tang, M.; Zhao, Y.N.; Hu, L.; Zhang, Y.Q.; Liang, Y.L. Crystallization of amorphous NiTi shape memory alloy fabricated by severe plastic deformation. *Trans. Nonferrous Met. Soc. China* **2014**, *24*, 1578–1765. [[CrossRef](#)]

11. Hua, P.; Wang, B.; Yu, C.; Han, Y.L.; Sun, Q.P. Shear-induced amorphization in nanocrystalline NiTi micropillars under large plastic deformation. *Acta Mater.* **2022**, *241*, 118358. [[CrossRef](#)]
12. Shahmir, H.; Nili-Ahmadabadi, M.; Huang, Y.; Jung, J.M.; Kim, H.S.; Langdon, T.G. Shape memory effect in nanocrystalline NiTi alloy processed by high-pressure torsion. *Mater. Sci. Eng. A* **2015**, *626*, 203–206. [[CrossRef](#)]
13. Pushin, V.G.; Valiev, R.Z.; Valiev, E.Z.; Kourov, N.I.; Kuranova, N.N.; Makarov, V.V.; Pushin, A.V.; Uksusnikov, A.N. Phase and structural transformation in the Ti<sub>49.5</sub>Ni<sub>50.5</sub> alloy with a shape-memory effect during torsion under high pressure. *Phy. Met. Metallogr.* **2012**, *113*, 256–270. [[CrossRef](#)]
14. Prokoshkin, S.D.; Khmelevskaya, I.Y.; Dobatkin, S.V.; Trubitsyna, I.B.; Tatyannin, E.V.; Stolyarov, V.V.; Prokofiev, E.A. Alloy composition, deformation temperature, pressure and post-deformation annealing effects in severely deformed Ti–Ni based shape memory alloys. *Acta Mater.* **2005**, *53*, 2703–2714. [[CrossRef](#)]
15. Huang, J.Y.; Zhu, Y.T.; Liao, X.Z.; Valiev, R.Z. Amorphization of TiNi induced by high-pressure torsion. *Phil. Mag. Lett.* **2004**, *84*, 183–190. [[CrossRef](#)]
16. Valiev, R.Z.; Gunderov, D.V.; Lukyanov, A.V.; Pushin, V.G. Mechanical behavior of nanocrystalline TiNi alloy produced by severe plastic deformation. *J. Mater. Sci.* **2012**, *47*, 7848–7853. [[CrossRef](#)]
17. Sergueeva, A.V.; Song, C.; Valiev, R.Z.; Mukherjee, A.K. Structure and properties of amorphous and nanocrystalline NiTi prepared by severe plastic deformation and annealing. *Mater. Sci. Eng. A* **2003**, *339*, 159–165. [[CrossRef](#)]
18. Gunderov, D.; Lukyanov, A.; Prokofiev, E.; Kilmametov, A.R.; Pushin, V.; Valiev, R. Mechanical properties and martensitic transformation in nanocrystalline Ti<sub>49.4</sub>Ni<sub>50.6</sub> alloy produced by high-pressure torsion. *Mater. Sci. Eng. A* **2009**, *503*, 75–77. [[CrossRef](#)]
19. Khmelevskaya, I.Y.; Prokoshkin, S.D.; Dobatkin, S.V.; Tatyannin, E.V.; Trubitsyna, I.B. Studies of composition, deformation temperature and pressure effects on structure formation in severely deformed TiNi-based alloys. *Mater. Sci. Eng. A* **2006**, *438–440*, 472–475. [[CrossRef](#)]
20. Ewert, J.C.; Böhm, I.; Peter, R.; Haider, F. The role of the martensite transformation for the mechanical amorphisation of NiTi. *Acta Mater.* **1997**, *45*, 2197–2206. [[CrossRef](#)]
21. Zhilyaev, A.P.; Langdon, T.G. Using high-pressure torsion for metal processing: Fundamentals and applications. *Procedia Mater. Sci.* **2008**, *53*, 893–979. [[CrossRef](#)]
22. Shuro, I.; Umamoto, M.; Todaka, Y.; Yokoyama, S. Phase Transformation and Annealing Behavior of SUS 304 Austenitic Stainless Steel Deformed by High Pressure Torsion. *Mater. Sci. Forum.* **2010**, *654*, 334–337.
23. Nakayama, H.; Tsuchiya, K.; Liu, Z.G.; Umamoto, M.; Mori, K.; Shimizu, T. Process of nanocrystallization and partial amorphization by cold rolling in TiNi. *Mater. Trans.* **2001**, *42*, 1987–1993. [[CrossRef](#)]
24. Razumov, I.K.; Yermalkov, A.Y.; Gormostyrev, Y.N.; Strauma, B.B. Nonequilibrium phase transformations in alloys under severe plastic deformation. *Physics-Uspokhi* **2020**, *63*, 733–757. [[CrossRef](#)]
25. Straumal, B.; Korneva, A.; Zieba, P. Phase transitions in metallic alloys driven by the high pressure torsion. *Arch. Civ. Mech. Eng.* **2014**, *14*, 242–249. [[CrossRef](#)]
26. Wang, X.B.; Verlinden, B.; Van Humbeeck, J. R-phase transformation in NiTi alloys. *Mater. Sci. Technol.* **2014**, *30*, 1517–1529. [[CrossRef](#)]
27. Waitz, T.; Karnthaler, H.P. Martensitic transformation of NiTi nanocrystals embedded in an amorphous matrix. *Acta Mater.* **2004**, *52*, 5461–5469. [[CrossRef](#)]
28. Waitz, T.; Antretter, T.; Fischer, F.D.; Karnthaler, H.P. Size effects on the martensitic phase transformation of NiTi nanograins. *J. Mech. Phys. Solids* **2007**, *55*, 419–444. [[CrossRef](#)]
29. Waitz, T.; Antretter, T.; Fischer, F.D.; Karnthaler, H.P. Size effects on the martensitic phase transformation of NiTi shape memory alloys. *Mater. Sci. Technol.* **2008**, *24*, 934–940. [[CrossRef](#)]
30. Shi, X.B.; Ma, Z.Y.; Zhang, J.S.; Ding, H.L.; Guo, F.M.; Liu, Y.; Cui, L.S. Grain size effect on the martensitic transformation temperatures of nanocrystalline NiTi alloy. *Smart Mater. Struct.* **2015**, *24*, 072001. [[CrossRef](#)]

**Disclaimer/Publisher’s Note:** The statements, opinions and data contained in all publications are solely those of the individual author(s) and contributor(s) and not of MDPI and/or the editor(s). MDPI and/or the editor(s) disclaim responsibility for any injury to people or property resulting from any ideas, methods, instructions or products referred to in the content.